RSC Mechanochemistry

ROYAL SOCIETY OF CHEMISTRY

PAPER

View Article Online
View Journal | View Issue

Cite this: *RSC Mechanochem.*, 2025, **2**, 246

Mechanochemical synthesis of eucairite CuAgSe and investigation of physicochemical and transport properties

Dáša Drenčaková, [ab] Marcela Achimovičová, *[a] Matej Baláž, [a] Jiří Navrátil, [c] Erika Tóthová,[a] Maksym Lisnichuk, [d] Jaroslav Briančin,[a] Viktor Puchý[e] and Tomáš Plecháček [c]

Copper silver selenide, CuAgSe, was easily and conveniently prepared from Cu, Ag and Se powders in a stoichiometric ratio by one-step solvent-free mechanochemical synthesis after 7 min of milling in a planetary ball mill. The kinetics of the synthesis, along with the structure, morphology, thermal stability, physicochemical, and thermoelectric properties of the product were investigated. The crystal structure, physicochemical properties, and morphology were characterised by X-ray diffraction, particle size distribution analysis, specific surface area measurements, X-ray photoelectron spectroscopy, and scanning and transmission electron microscopy. XRD confirmed the crystal structure as a mixture of tetragonal and orthorhombic CuAgSe. Analysis of surface composition revealed partial surface oxidation. Electron microscopy revealed that the nanostructured product consisted of agglomerated particles of irregular shape which formed clusters with a size >20 μm while the mean size of crystallites was 12.1 nm. The mixed crystal structure was also confirmed by selected area diffraction. Thermal analysis clearly indicated a reversible phase transformation. The spark plasma sintering method was applied to prepare a dense CuAgSe pellet for thermoelectric characterization. High-temperature transport properties were examined to assess the potential application of mechanochemically synthesized synthetic eucairite in energy conversion.

Received 28th September 2024
Accepted 3rd December 2024

DOI: 10.1039/d4mr00111g

rsc.li/RSCMechanochem

Introduction

Copper and silver chalcogenides are considered promising materials for various applications, such as thermoelectrics,[1,2] photovoltaics[3] or superconductors,[4] thanks to their physicochemical properties. Essential properties for their use as thermoelectric materials are their very high carrier mobility and reduced thermal conductivity.[5] Eucairite – CuAgSe, a ternary copper(I) silver selenide belongs to a group of interesting metal chalcogenides. The earliest investigation of its crystal structure determined that the only tetragonal structure is β-CuAgSe.[6] However, a few years later another study showed that β-CuAgSe crystallizes in pseudo-tetragonal orthorhombic symmetry with a large supercell.[7] Based on recent knowledge there are three modifications of ternary copper(I) silver selenide (see Fig. 1), namely, low-temperature tetragonal β-CuAgSe, low-temperature orthorhombic β-CuAgSe, and high-temperature cubic α-CuAgSe, with the temperature of phase transition between low- and high-temperature modifications being approximately 504 K.[8] Furthermore, the existence of a reversible phase transition in the temperature range of 463–468 K between low- and high-

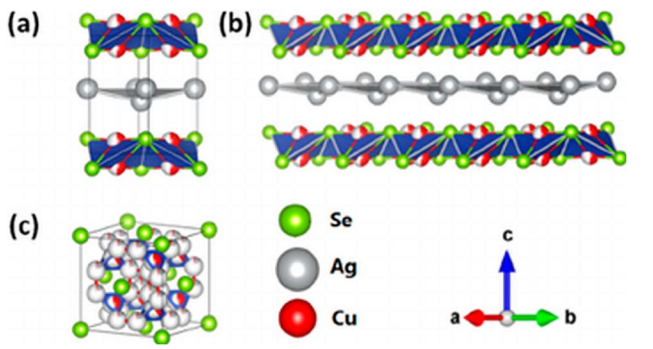

Fig. 1 CuAgSe crystal structure scheme: (a) tetragonal, (b) orthorhombic and (c) cubic. Reprinted with permission from C. Han, Q. Sun, Z. X. Cheng, J. L. Wang, Z. Li, G. Q. Lu and S. X. Dou; "Ambient scalable synthesis of surfactant-free thermoelectric CuAgSe nanoparticles with reversible metallic-n–p conductivity transition," *J. Am. Chem. Soc.*, 2014, 136, 17626, DOI: 10.1021/ja510433j. Copyright 2014 American Chemical Society.

[a]*Institute of Geotechnics, Slovak Academy of Sciences, Košice, Slovakia. E-mail: achimovic@saske.sk*
[b]*Institute of Metallurgy, Technical University of Košice, Slovakia*
[c]*University of Pardubice, Faculty of Chemical Technology, Pardubice, Czech Republic*
[d]*Faculty of Science, P. J. Šafárik University, Košice, Slovakia*
[e]*Institute of Materials Research, Slovak Academy of Sciences, Košice, Slovakia*

temperature CuAgSe modifications was found.[7] The cubic α-phase has been described as a rigid fcc lattice of Se anions with mobile, randomly distributed Ag and Cu cations responsible for the superionic behaviour.[9] Depending on the type of charge carriers, n-type and p-type semiconductors can be distinguished. A unique feature of CuAgSe is its ability to switch between both types of conductivity, connected with phase transition.[1] In order to maintain n-type behaviour over a broad temperature range, CuAgSe can be doped with Te,[10] Ni,[11] Co, and Zn.[12]

Chemical compounds derived from the rare mineral eucairite have been synthesized and studied by many different methods. For the preparation of CuAgSe, mostly solid-state reactions have been used. The most commonly used methodology encompasses the loading of powdered elemental precursors into an evacuated silica tube and heating them to temperatures above 1173 K.[13–16] Other methods of CuAgSe synthesis are chemical precipitation,[1,17,18] conversion of $Cu_{2-x}Se$,[3] manual mixing of the elements followed by spark plasma sintering,[19] solvothermal synthesis,[20] magnetron sputtering,[21] and mechanical alloying in a planetary ball mill.[2,4,22] Among the abovementioned synthesis methods, mechanochemical reaction provides numerous benefits, because it is a simple, one-step, one-pot, time-saving, economical and environmentally friendly method. In contrast to chemical precipitation, mechanochemical reaction proceeds without the use of any solvent and unlike solid-state reactions, it is carried out at ambient pressure and temperature. Additionally, the mechanochemical process enables a transfer to large-scale industrial production.[23,24] The first reported mechanochemical synthesis of CuAgSe was performed by high-energy milling of elemental powder precursors in a planetary ball mill for 60 minutes.[4] In a more recent study, milling of precursors in the planetary ball mill proceeded for 16 h, and the effect of chemical composition on structural stability, and thermoelectric performance was investigated.[2] Different ball-to-powder ratios and milling atmospheres, but the same milling time, 16 h, were applied in the most recent study, which was focused on thermoelectric properties and the control of n–p conduction type transition.[22] In all cases, the material used for the milling chamber and balls was agate.

In the present study, tungsten carbide (WC) milling media were used leading to a very fast mechanochemical synthesis of nanostructured CuAgSe by high-energy milling in a planetary ball mill. The novelty lies in the very short time required to obtain the desired product, which was only 7 minutes. The kinetics of the mechanochemical synthesis of synthetic mineral eucairite was studied, and its crystal structure, morphology, physicochemical, and thermoelectric properties were also investigated.

Experimental

The mechanochemical synthesis of CuAgSe was performed using a Pulverisette 6 planetary ball mill (Fritsch, Germany), according to the reaction: Cu + Ag + Se → CuAgSe. The precursors used for synthesis were powders of elemental copper (99%, 116 μm, Nippon Atomized Metal Powders Corp. Japan), silver (99,9%, 125 μm, Thermo Scientific Chemicals) and selenium (99,5%, 74 μm, Acros Organics). The amounts of each precursor were calculated to yield 5 g of CuAgSe, namely, 1.27 g Cu, 2.15 g Ag and 1.58 g Se. The following milling conditions were used: a 250 mL milling chamber loaded with 50 pieces of balls (10 mm in diameter), WC as the material for both the milling chamber and balls, a ball-to-powder weight ratio of 73 : 1, an inert Ar atmosphere, a rotation speed of 550 rpm and various milling times, $t_M = 1$, 3, 5, 7 min.

The products of the mechanochemical reaction with different milling times, t_M, were characterized by the following techniques. Qualitative X-ray diffraction analysis (XRD) was performed using a D8 Advance diffractometer (Bruker, Germany), working in Bragg–Brentano geometry with CuK_α as the radiation source ($\lambda = 0$, 154 nm) at 40 mA and 40 kV. The data were analysed using JANA2020 software; for modelling of diffraction lines, a pseudo-Voigt function was used. The present phases were identified according to the JCPDS PDF database.

The particle size distribution (PSD) was measured using a Mastersizer 2000E particle size laser diffraction analyzer (Malvern Panalytical, UK) with a Scirocco 2000M dry feeder and a measurement range of 0.02–2000 μm.

The Brunauer–Emmett–Teller (BET) specific surface area values, S_{BET}, were assessed by the low-temperature nitrogen adsorption method in a Gemini 2360 sorption apparatus (Micromeritics, USA) with an applicability of 0.01 $m^2\ g^{-1}$, in the pressure range of 0–950 mm Hg, and with accuracy and linearity better than ±0.5%.

For X-ray photoelectron spectroscopy (XPS), the powder samples were fixed with a double-adhesive carbon tape on a stainless sample holder. The measurements were performed using a ULVAC-PHI Quantes (Japan) with a monochromatic Al Kα source at 1486.6 eV. Three areas with a spot size of ~100 μm were analysed. The photoelectrons were collected at an emission angle of 45°. The high-resolution spectra were obtained at 55 eV pass energy and 0.1 eV step size. The X-ray source was set to 25 W and 15 kV. The carbon C 1s peak at 284.8 eV was used as an internal reference for charge correction. The charge compensation was performed with low-energy Ar^+ ions and electrons.

Scanning electron microscopy (SEM) analysis was performed using a MIRA 3 FE-SEM microscope (TESCAN, Czech Republic), equipped with an energy dispersive X-ray spectroscopy (EDX) detector (Oxford Instruments, UK).

Transmission electron microscopy (TEM) was performed using a JEOL 2100F UHR operating at 200 kV with a field emission gun. Image characterization was done in scanning/transmission mode employing a bright field detector. Phase identification was confirmed by the selected area electron diffraction (SAED) technique. The studied sample was dispersed in ethanol and ultrasonicated for 15 min before observation to reduce agglomeration. This sample dispersion was placed on a copper support grid covered with an ultra-thin flat carbon film and stored in a vacuum.

The thermal behaviour was investigated by TG/DTG/DTA measurements using an STA 449 F3 Jupiter thermal analyzer

(Netzsch, Germany). The measurements were performed over the temperature range of 25–300 °C at a heating rate of 10 °C min^{-1} under an argon 5.0 (purity 99.999%) atmosphere with a constant flow of 30 mL min^{-1}. As the reference material, an Al_2O_3 crucible was used.

The CuAgSe sample for transport property measurements was sintered by the spark plasma sintering method (SPS) in an HP D10-SD furnace (FCT Systeme GmbH, Germany). The powder was placed into a graphite die (inner diameter 10 mm) and sintered into a round pellet about 2 mm thick at 673 K under 80 MPa (heating rate 100 K min^{-1}), with a holding time of 10 min in an Ar atmosphere. The electrical conductivity, σ, was measured *via* the four-terminal method using an LSR-3 instrument (Linseis, Germany) from 300 to 624 K on a round pellet. The Seebeck coefficient, S was measured *via* the static DC method using an LSR-3 instrument, and the electrical conductivity was measured simultaneously with the Seebeck coefficient. The measurements were performed in a He atmosphere under 0.1 bar overpressure. The thermal diffusivity, k was measured from 300 to 574 K on a round pellet using an LFA 457 instrument (Netzsch, Germany). The thermal conductivity, κ was subsequently calculated using the relation $\kappa = k \times c_p \times \rho$, where k is the thermal diffusivity, c_p is the heat capacity, and ρ is the experimental density. Super-alloy Inconel was used as the heat-capacity standard. The thermoelectric figure of merit, ZT, was calculated according to the equation $ZT = \sigma S^2 T/\kappa$.

The Hall coefficient was measured up to 625 K in an Ar atmosphere using a home-made cell. The method used an alternating current at a frequency of 1020 Hz and a stationary magnetic field with an induction of 0.4 T. Welded platinum-wire voltage contacts and mechanically applied pressure current contacts were used.

Results and discussion

XRD patterns of stoichiometric Cu/Ag/Se mixtures milled for various milling times t_M, representing the kinetics of the mechanochemical reaction, are shown in Fig. 2. The XRD patterns of the mixtures treated for 1 and 3 min exhibited diffraction peaks corresponding to unreacted elemental Cu (03-065-9026) and the reaction intermediate Ag_2Se (01-080-7685). Also, a small amount of synthetic eucairite CuAgSe was detected, indicating that its formation started already after 1 min of milling. These results suggest that the mechanochemical reaction was indirect and proceeded *via* two steps: first Ag_2Se was formed, followed by CuAgSe formation. A similar rection pathway was reported for the synthesis of CuAgSe nanoparticles *via* the precipitation route, where Cu^+ ions replace Ag^+ ions in Ag_2Se to create CuAgSe.[18] The most appropriate t_M was 7 min because, in the sample with $t_M = 5$ min, unreacted Cu and/or intermediate Ag_2Se in concentrations below the detection limit (up to 5 wt%) could still be identified. As t_M increased, complete conversion of the precursors and intermediate into the desired product CuAgSe occurred. XRD phase analysis found that the product with $t_M = 7$ min contained a mixture of orthorhombic (CuAgSe, 00-010-0451) and tetragonal (CuAgSe, 01-089-3935) modification of eucairite. The XRD pattern contained some extra peaks, which according to the literature[4] belong to the orthorhombic phase of CuAgSe.

The assignment of the CuAgSe structure is complicated due to discrepancies in the literature; some researchers supposed that there is only one pseudo-tetragonal orthorhombic structure[4,13] while others assumed the coexistence of tetragonal and orthorhombic structures.[1,2,19,22] Another complication could be the presence of impurities, such as oxidized by-products. Le Bail refinement was performed on the Cu/Ag/Se mixture treated for 7 min starting with the cell parameters of the orthorhombic structure, a = 4.105 Å, b = 4.07 Å, and c = 6.31 Å, and the tetragonal structure, a = 4.105 Å, b = 4.105 Å, and c = 6.31 Å. Between them, there is only a little difference in the b-axis, which does not have a significant effect on electronic properties.[25] To achieve the best fit, two phases with the following slightly different cell parameters were obtained based on the least-square refinement results: $a = 4.0976$ Å, $b = 20.6916$ Å, and $c = 6.4178$ Å, and $a = 4.1621$ Å, $b = 20.7545$ Å, and $c = 6.5323$ Å for the orthorhombic and tetragonal structure, respectively. A large supercell $a \times 5b \times c$ (ref. 7) was detected. The statistics of the refinement along with the graphical output are given in Fig. 3. The estimation of crystallite size was not possible due to overlapping peaks of the two nearly identical phases.

The results of PSD analysis and S_{BET} values of Cu/Ag/Se mixtures with various milling times t_M are illustrated in Fig. 4. The smooth PSD curve of Cu/Ag/Se milled for 7 min indicated a monomodal particle size distribution with the most uniform particles, in contrast to the Cu/Ag/Se mixtures milled for 1, 3, and 5 min. This supported the XRD results, confirming the completion of the mechanochemical reaction after 7 min of milling (see Fig. 4a). Fig. 4b shows the dependencies of the mean particle size values, $d(0.5)$, calculated from PSD analysis and S_{BET} values on t_M. The course of the S_{BET} curve is similar to that observed for mechanochemically synthesized materials, especially chalcogenides described in the literature.[26] A maximum S_{BET} value of 0.55 $m^2\ g^{-1}$ was reached for the mixture with t_M = 3 min, which suggests that at first, new surfaces

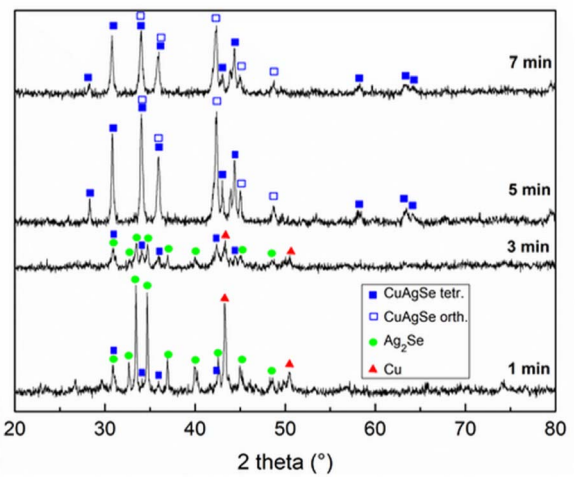

Fig. 2 XRD patterns of Cu/Ag/Se mixtures at milling times, t_M = 1, 3, 5, 7 min.

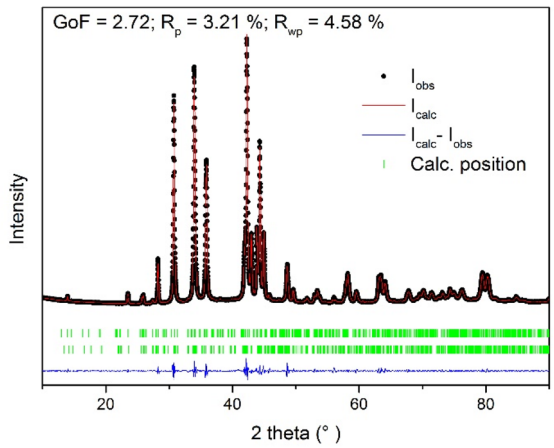

Fig. 3 The graphical Le Bail refinement output of the orthorhombic cell parameters against the measured data of the Cu/Ag/Se mixture milled for 7 min.

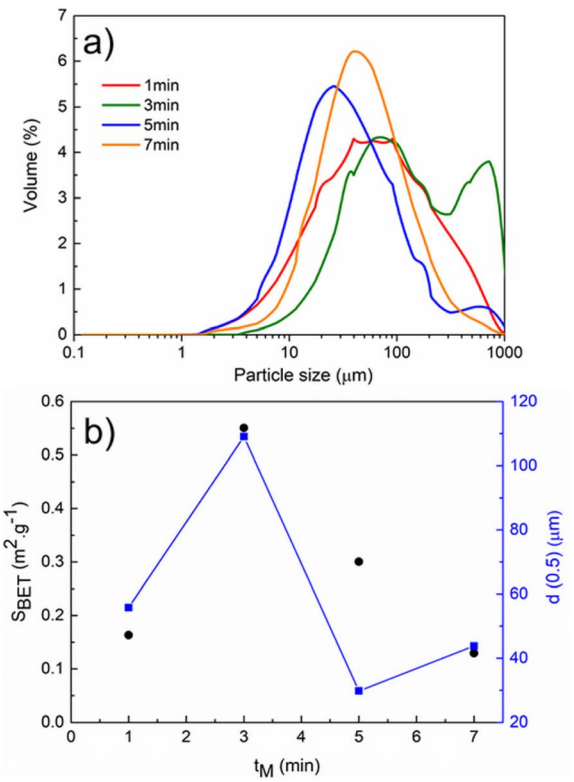

Fig. 4 (a) Particle size distribution of Cu/Ag/Se mixtures and (b) dependence of specific surface area, S_{BET} and particle size $d(0.5)$ of milled Cu/Ag/Se mixtures on the time of mechanochemical synthesis, t_M.

among the reactants and intermediate phases were formed and only then the reaction proceeded to a large extent. The formation of the final CuAgSe product is accompanied by a decrease in the S_{BET} value down to 0.14 $m^2\ g^{-1}$ for the Cu/Ag/Se mixture milled for 7 min because the product particles agglomerated. The lowest mean particle size $d(0.5) = 29.77$ μm was achieved for the 5 min-milled mixture, while a higher value of $d(0.5) = 43.79$ μm was measured for the final CuAgSe product, which also demonstrated the effect of particle agglomeration – a common phenomenon occurring in the mechanochemical synthesis of chalcogenides.[27–30]

XPS analysis was performed to evaluate the surface chemical state of the synthesized CuAgSe product milled for 7 min. The detailed XPS spectral lines of Cu 2p, Ag 3d and Se 3d are presented in Fig. 5. The binding energy (BE) value of 932.6 eV (see Fig. 5a) corresponded to the Cu $2p_{3/2}$ fitted spectral line of Cu^+ species,[1,27] which overlapped with the fitted spectral line of Cu^{2+} species (BE = 934.2 eV). Also, the presence of the typical Cu^{2+} satellite with a BE of around ~941–944 eV indicated slight surface oxidation of the product and the formation of CuO.[31,32] Such surface oxidation of Cu^+ to Cu^{2+} due to storage and handling in the air atmosphere was observed for CuAgSe nanotubes and Cu_2Se nanoparticles as a result of the high density of surface sites.[33,34] In Fig. 5b, the BEs of 373.9 eV and

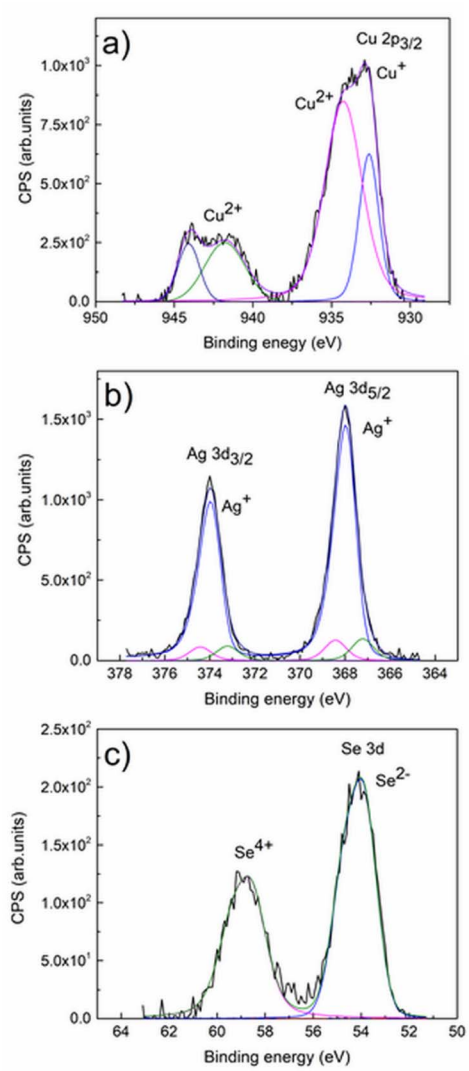

Fig. 5 XPS spectra of mechanochemically synthesized CuAgSe: (a) Cu 2p; (b) Ag 3d; (c) Se 3d.

367.8 eV for Ag $3d_{3/2}$ and Ag $3d_{5/2}$ spectral lines, respectively, are in accordance with other data published for CuAgSe and confirm the Ag^+ valence state.[33] The overlapped spectral lines of Se $3d_{5/2}$ and Se $3d_{3/2}$ are dominated by the peak with a BE of around 54 eV (Fig. 5c), which can be satisfactorily assigned to the Se(-II) oxidation state of selenium. The broad peak located at a slightly higher energy level with BE = 58 eV probably belongs to SeO_2 which also indicates partial surface oxidation of the CuAgSe product.

The morphology of the milled mixtures for 3 min and 7 min was studied using SEM-EDX. The observations corresponded with the results of PSD and XRD analysis. Even after 3 min of milling, the overall morphology of the mixture supported the fast conversion of elemental precursors. However, unreacted copper metal, also detected by XRD analysis, can be seen in Fig. 6a as detected by EDX elemental mapping analysis (shown in red). The Ag_2Se intermediate product revealed by XRD could not be satisfactorily spotted by EDX analysis. Both mixtures consisted of agglomerated particles of irregular shape. In the final CuAgSe product with t_M = 7 min, shown in Fig. 6b, no particles of unreacted precursors were found and the individual elements Cu, Ag, and Se were homogeneously distributed. The

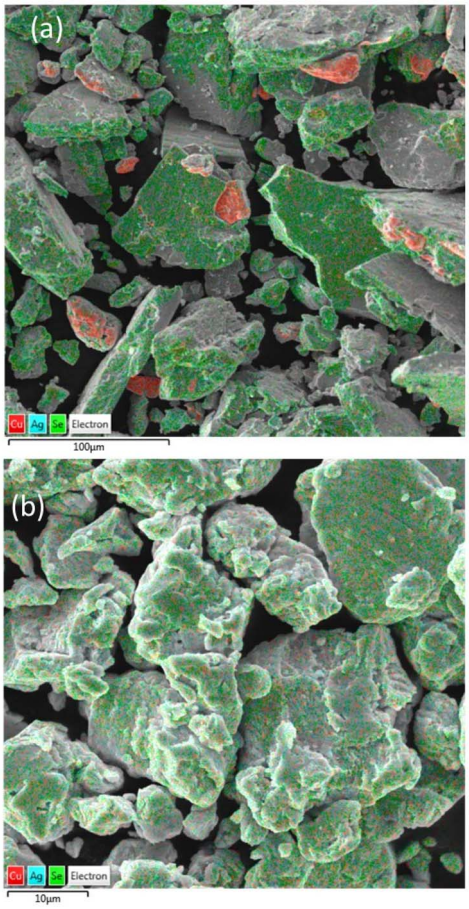

Fig. 6 SEM micrographs with elemental mapping of Cu/Ag/Se mixtures milled for (a) 3 min and (b) 7 min.

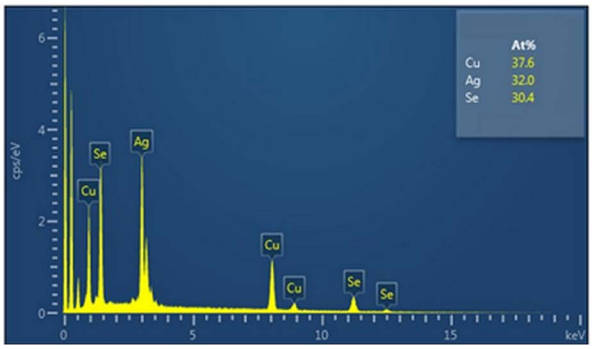

Fig. 7 EDX analysis of CuAgSe milled for 7 min.

average at% composition of Cu : Ag : Se was 1.1 : 0.96 : 0.91, as confirmed by EDX analysis (see Fig. 7).

The results of TEM analysis of CuAgSe milled for 7 min showed a cluster of agglomerated particles in bright-field STEM mode (see Fig. 8a). Analysis of the SAED pattern in Fig. 8b confirmed a very good agreement with the CuAgSe phase crystallizing in the tetragonal (space group: *P4/nmm* [129]; a = 0.408 nm, c = 0.631 nm) and orthorhombic crystallographic systems (space group: *Pmmn* [59]; a = 0.41 nm, b = 0.407 nm, c = 0.631 nm), which correspond to the values obtained from XRD analysis.

The PSD of the CuAgSe particles was determined by analyzing many images taken in bright-field STEM mode. The observation mode was set to avoid unwanted diffraction effects. The result, shown as a skewed right histogram in Fig. 9, confirmed that particles with a size of up to 55 nm were observed. The average physical size of the particles was determined by fitting of a Gaussian function to the particle size distribution estimated from TEM micrographs. The calculated mean crystallite size was 12.1 nm.

The thermal analysis of the CuAgSe product with t_M = 7 min, *i.e.*, the final CuAgSe product, measured in reversible mode

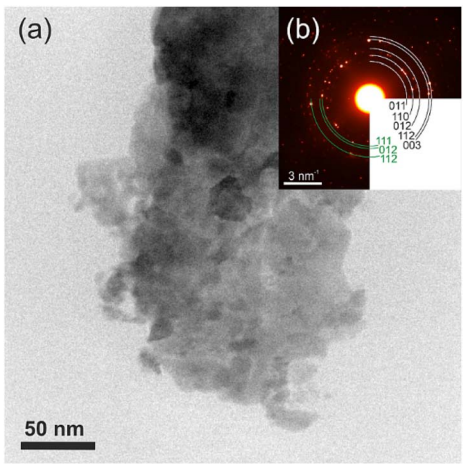

Fig. 8 TEM images of (a) agglomerated crystals of CuAgSe milled for 7 min; (b) SAED pattern of the same crystals (tetragonal phase – black and orthorhombic phase – green).

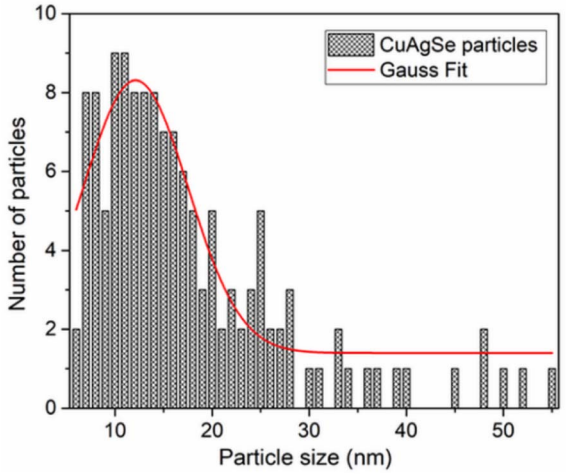

Fig. 9 Particle size distribution analysis of CuAgSe agglomerated crystals from TEM observation.

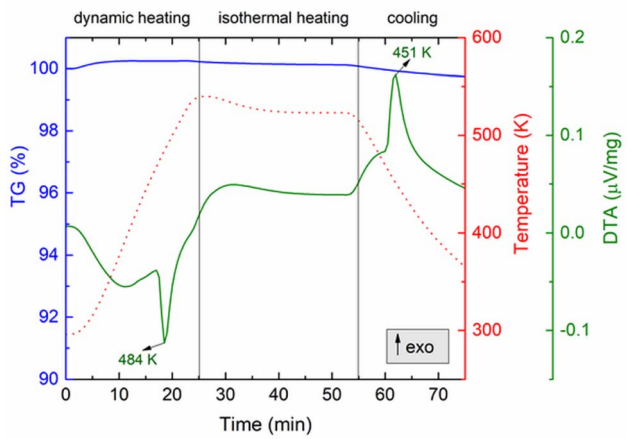

Fig. 10 Thermal analysis of the CuAgSe product (t_M = 7 min) with phase transition.

(heating–cooling), is shown in Fig. 10. As can be seen, there is no weight loss on the TG curve, confirming the stability of the mechanosynthesized CuAgSe; however, two important peaks are visible on the DTA curve indicating phase transformations. The first endothermic peak at 484 K observed during the heating mode is associated with the phase transition from low-temperature β-CuAgSe to high-temperature α-CuAgSe,[8,9] which confirmed the low-temperature phase formation during milling. During cooling, the reversible process can be observed as an exothermic peak at 451 K. It should be mentioned that although the reversible phase transformation during cooling occurred at the same temperature as during heating, the shift of the peak maximum to a lower temperature is related to lattice distortion, stress, and differences in cell volumes before and after the transformation, which requires a certain time period. However, compared to the literature,[35] there is a small shift in the peak maxima as well, *i.e.*, a higher temperature during heating and a lower temperature during cooling, indicating a more disordered structure as a result of the mechanochemical preparation procedure.

The XRD pattern of this cooled product after thermal treatment shown in Fig. 11 confirmed recrystallization to the original CuAgSe product containing a mixture of both crystal phases. However, an amorphous phase has also been detected, indicating the presence of an amorphous glassy state in the originally mechanosynthesized product which was not detected by XRD. The XRD pattern of the pellet after SPS treatment similarly identified recrystallized CuAgSe together with amorphous phase formation.

The quality of the mechanochemically prepared β-CuAgSe was also evaluated in terms of the thermoelectric material potential. Thermoelectric properties were studied in the temperature range from 300 to 624 K. A significant change in the temperature dependence of electrical conductivity σ, Seebeck coefficient S, thermal conductivity κ, and ZT was related to phase transition, which occurred between 460 and 500 K (see Fig. 12a–d). According to the temperature-dependent data of σ shown in Fig. 12a, one can observe rather high metallic conductivity of the β-phase, while after the phase transition, σ decreases and a semiconducting character of σ is observed for the α-phase material with increasing temperature.

The observed metallic behaviour of the β-phase is in good agreement with previous theoretical calculations.[1,5] These calculations also show that two types of carriers (electrons and holes) should contribute to the electrical conduction. The measurements of the Seebeck coefficient S (see Fig. 12b) and the Hall coefficient R_H (Fig. 13 inset) reveal the dominant role of electrons in the low-T region, *i.e.*, before the phase transition. The almost constant Hall concentration ($\sim 4 \times 10^{18}$ cm^{-3}) and rather high increasing Seebeck values with rising temperature indicate very little participation of holes in the electric transport in this region. This fact is also reflected by very high Hall mobilities μ_H (see Fig. 13) at 300 K ($\sim$1600 cm^2 V^{-1} s^{-1}). The unusually high value of the n-exponent in the μ_H–T^n (n = 2.75) dependence for the β-phase suggests that the dominant scattering mechanism on homopolar optical phonons occurs in the

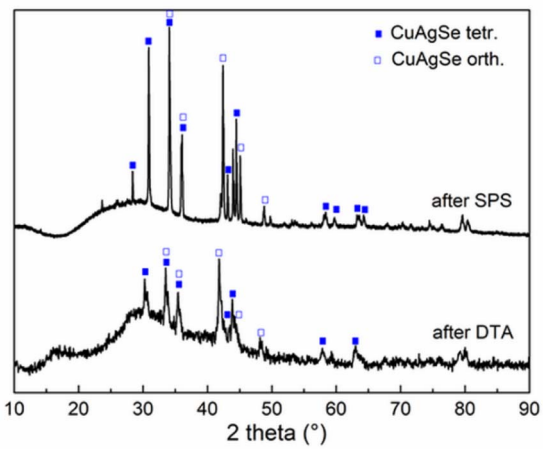

Fig. 11 XRD pattern of CuAgSe milled for 7 min after thermal treatment by SPS (400 °C) and DTA (300 °C).

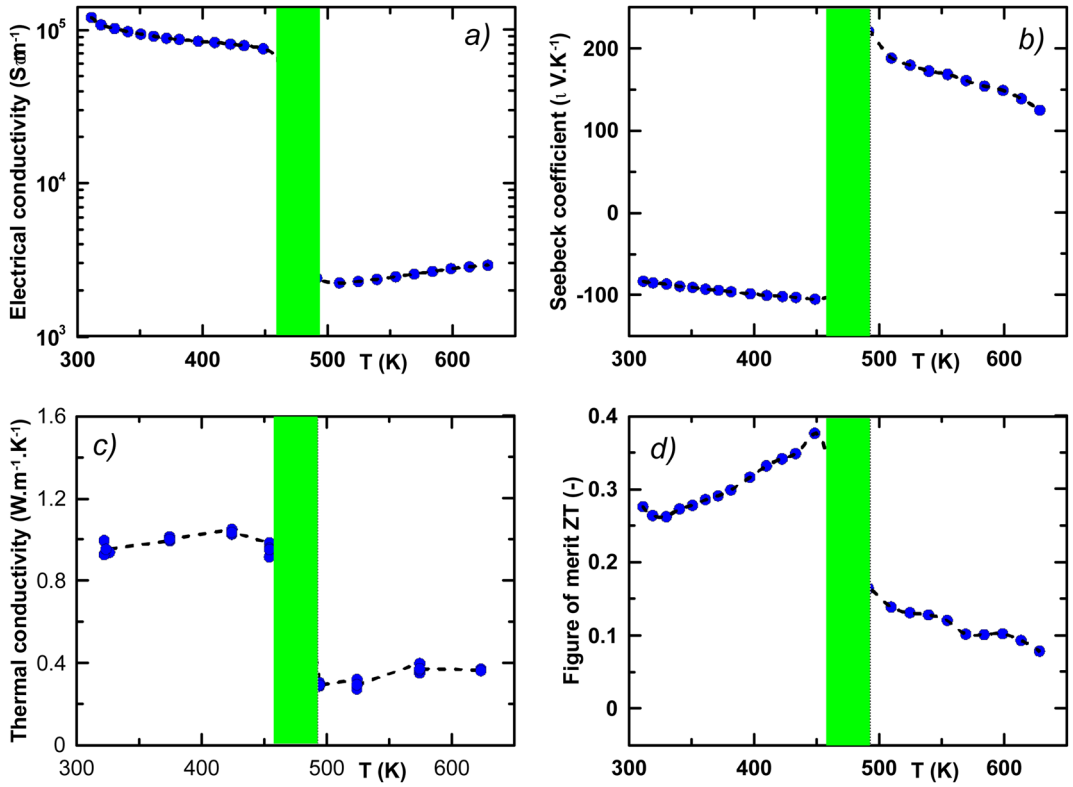

Fig. 12 Thermoelectric properties of CuAgSe, temperature-dependent (a) electrical conductivity σ, (b) Seebeck coefficient S, (c) thermal conductivity κ, and (d) thermoelectric figure of merit ZT. Semitransparent green rectangles represent the area of α to β phase transition.

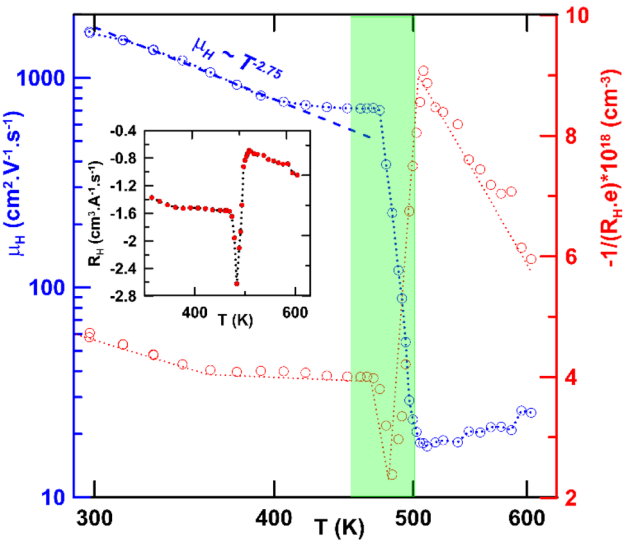

Fig. 13 Log–log plot of the Hall mobility m_H and the Hall concentration $1/(R_H \times e)$ as a function of T. In the inset, R_H *vs.* T is presented. The semitransparent green rectangle represents the area of β to α phase transition.

area which is intrinsic to layered materials.[36–38] Drastic changes in the measured transport properties after the β–α phase transition at $T > 500$ K connected with the transformation to a semiconducting phase can be explained by a sudden increase in hole concentration in the α-phase material. The holes are generated mainly by the disordered Cu and Ag ions in the high-T cubic structure. Although the S-values for the α-phase suddenly change to positive ones, surprisingly the R_H remains negative in the region. It indicated that a rather high concentration of electrons is present in the system. This can be explained within the context of a two-carrier model. The Seebeck coefficient S and the Hall coefficient R_H can be described within the frame of the model:

$$S = \frac{S_e \times \sigma_e + S_h \times \sigma_h}{\sigma_e + \sigma_h} \quad (1)$$

and

$$R_H = \frac{n_e \times \mu_e^2 - n_h \times \mu_h^2}{e \times (n_e \times \mu_e + n_h \times \mu_h)^2}, \quad (2)$$

where S_e, S_h, σ_e, σ_h, n_e, n_h, μ_e, and μ_h, are the Seebeck coefficient (S), electrical conductivity (σ), carrier concentration (n) and carrier mobility (μ) for electrons (e) and holes (h), respectively. Thus, in the case of $\mu_e \gg \mu_h$, the values of R_H can still be negative even when hole concentration dominates over electron concentration. Such domination leads to positive values of S. The decrease in total thermal conductivity after phase transition happened due to a decrease in electronic thermal conductivity, which is associated with a decrease in electrical conductivity (see Fig. 12c). Lattice thermal conductivity did not change significantly throughout the whole temperature range, except for the highest value observed at 474 K. The

Table 1 Overview of ZT values of β-CuAgSe before phase transition prepared by various methods with different conditions

Method of preparation	Synthesis conditions: temperature/time	Max. ZT	Year/Ref.
Chemical precipitation	RT[a]/25 min	0.42	2014/[1]
Solid state reaction	1373 K/12 h	0.62	2015/[10]
Solid state reaction	1253 K/54 h	0.10	2015/[13]
Manual mixing & SPS	RT/10 min & 673 K/10 min	0.60	2016/[19]
Ball milling[b]	RT/16 h	0.45	2018/[2]
Solid state reaction	Not available	0.50	2019/[39]
Solid state reaction	1373 K/20 h	0.30	2019/[11]
Solid state reaction	1323 K/130 h	0.29	2021/[12]
Solid state reaction	1323 K/165 h	0.24	2023/[40]
Ball milling[b]	RT/16 h	0.25	2023/[22]
Manual mixing & SPS	RT/30 min & 30 s	0.35	2024/[41]
Ball milling[b]	RT/7 min	0.35	This study

[a] Room temperature. [b] Product prepared before any thermal treatment, SPS followed only in order to consolidate powder.

thermoelectric figure of merit illustrated in Fig. 12d reached the highest value $ZT = 0.35$ at 424 K before phase transition.

Compared with the recently published results for other low-temperature β-CuAgSe compounds prepared by ball milling, the maximum ZT values achieved are in quite good agreement with our ZT values while the time required for the mechanochemical synthesis presented here was several times shorter (see Table 1). Additionally, Table 1 summarizes the preparation conditions of β-CuAgSe by different methods and their corresponding ZT values published in the last 10 years.

Table 1 shows that the predominant preparation method was the solid-state reaction technique, which is demanding in terms of thermal energy and time. The unconventional one-pot and one-step mechanochemical method carried out at room temperature is also presented here, evidencing that was the fastest under the given conditions. Although it appears that the preparation of CuAgSe by manual mixing is advantageous, it should be noted that in this case, no CuAgSe product was formed even after 10 or 30 min of manual mixing, with the product only forming after the SPS procedure. In general, mechanochemistry is considered one of the sustainable, environmentally promising technologies with good green chemistry metrics.[42] The main advantage of mechanochemical synthesis is its easy scalability using large-scale industrial mills, capable of producing up to tons of material per year with the possibility of achieving the required technology readiness level.[24] Further research and testing of mechanochemical synthesis for its implementation in the chemical industry is still needed for verification.

Conclusions

The ternary copper silver selenide – synthetic mineral eucairite was prepared using energy-saving and "green" mechanosynthesis in a planetary ball mill. Monitoring of the kinetics of the mechanochemical reaction using XRD confirmed its completion after 7 min of milling. The synthesized CuAgSe had mixed tetragonal and orthorhombic crystal structures determined by XRD and Rietveld refinement. This mixed structure was additionally confirmed by TEM and SAED analyses which revealed agglomerated nanocrystals with a crystallite size of 12 nm. The PSD curve of the powdered product corresponded to a monomodal particle size distribution with $d(0.5)$–44 μm. The reduction of the S_{BET} value to 0.14 $m^2\ g^{-1}$ and the increase in $d(0.5)$ compared to unreacted mixtures was a consequence of the formation of the resulting product and the simultaneous agglomeration. Oxidation states of Cu^+, Ag^+, and Se^{2-} in CuAgSe were confirmed by XPS analysis, which also indicated slight surface oxidation of the product. The thermal analysis demonstrated the reversible phase transition from low-temperature β-CuAgSe prepared by milling, to high-temperature α-CuAgSe. During cooling, the cubic α-CuAgSe recrystallized into the original mixture of tetragonal and orthorhombic β-CuAgSe, but with some content of the amorphous phase. Furthermore, the thermoelectric performance of the synthesized product was evaluated and compared with the reported ZT values. Through this research, it was found that by appropriately setting the milling conditions, the CuAgSe synthesis time could be significantly shortened to 7 min, while the thermoelectric performance remained comparable. Moreover, this synthesis method presents a suitable alternative to the existing methods of CuAgSe production. From our previous research and experience, it is evident that this type of synthesis can be easily adapted to production scales using an industrial vibratory mill.

Data availability

The authors declare that the data supporting the findings of this study are available within the paper. Should any raw data files be needed in another format they are available from the corresponding author upon reasonable request. Source data are provided in this paper.

Author contributions

Conceptualisation: D. D. and M. A.; investigation: D. D., M. A., M. B., E. T., J. N., V. P., and T. P.; formal analysis: D. D., M. B., E. T., and J. N., visualisation: J. B., M. L., and J. N.; writing-original draft: M. A., D. D., writing review and editing: M. A., D. D., and J. N.

Conflicts of interest

There are no conflicts to declare.

Acknowledgements

This work was realized within the Slovak Grant Agency (VEGA 02/0036/23). The authors would like to thank Dr R. Bureš from the Institute of Materials Research, Slovak Academy of Sciences (Košice, Slovakia) for performing the PSD analyses, and Dr Jörg Radnik from the Federal Institute of Materials Research and Testing (Berlin, Germany) for performing the XPS measurements.

References

1 C. Han, Q. Sun, Z. X. Cheng, J. L. Wang, Z. Li, G. Q. Lu and S. X. Dou, Ambient scalable synthesis of surfactant-free thermoelectric CuAgSe nanoparticles with reversible metallic- n–p conductivity transition, *J. Am. Chem. Soc.*, 2014, **136**, 17626–17633, DOI: 10.1021/ja510433j.

2 A. Olvera, T. P. Bailey, C. Uher and P. F. P. Poudeu, Chemical manipulation of phase stability and electronic behavior in $Cu_{4-x}Ag_xSe_2$, *J. Mater. Chem. A*, 2018, **6**, 6997–7004, DOI: 10.1039/C8TA01531G.

3 S. Gahlot, F. Dappozze, D. Singh, R. Ahuja, L. Cardenas, L. Burel, D. Amans, C. Guillard and S. Mishra, Room-temperature conversion of $Cu_{2-x}Se$ to CuAgSe nanoparticles to enhance the photocatalytic performance of their composites with TiO_2, *Dalton Trans.*, 2020, **49**, 3580–3591, DOI: 10.1039/C9DT0472.

4 T. Ohtani, K. Maruyama and K. Ohshima, Synthesis of copper, silver, and samarium chalcogenides by mechanical alloying, *Mater. Res. Bull.*, 1997, **32**, 343–350, DOI: 10.1016/S0025-5408(96)00188-2.

5 S. Ishiwata, Y. Shiomi, J. S. Lee, M. S. Bahramy, T. Suzuki, M. Uchida, R. Arita, Y. Taguchi and Y. Tokura, Extremely high electron mobility in a phonon-glass semimetal, *Nat. Mater.*, 2013, **12**, 512–517, DOI: 10.1038/nmat3621.

6 J. W. Earley, Description and synthesis of the selenide minerals, *Am. Mineral.*, 1950, **35**, 337–364.

7 A. J. Frueh, G. K. Czamanske and Ch. Knight, The crystallography of eucairite, CuAgSe, *Z. Kristallogr.*, 1957, **108**, 389–396, DOI: 10.1524/zkri.1957.108.5-6.389.

8 K. Kiazimov, K. M. Jafarov and Y. G. Asadov, Structural phase transitions in (Ag, Cu)S, Se, Te crystals, *Phase Transitions*, 1990, **21**, 11–21, DOI: 10.1080/01411599008206878.

9 T. Shimoyama, M. Arai and T. Sakuma, *Crystal Structure of the Superionic Phase of CuAgSe, Superionic Conductor Physics*, WORLD SCIENTIFIC, Kyoto, Japan, 2007, pp. 27–30, DOI: 10.1142/9789812706904_0005.

10 P. F. Qiu, X. B. Wang, T. S. Zhang, X. Shi and L. D. Chen, Thermoelectric properties of Te-doped ternary CuAgSe compounds, *J. Mater. Chem. A*, 2015, **3**, 22454–22461, DOI: 10.1039/C5TA06780D.

11 J. Y. Zhang, J. H. Zhu, L. You, K. Guo, Z. L. Li, W. G. Lin, J. Huang and J. Luo, Enhanced and stabilized n-type thermoelectric performance in α-CuAgSe by Ni doping, *Mater. Today Phys.*, 2019, **10**, 100095, DOI: 10.1016/j.mtphys.2019.100095.

12 T. H. Nguyen, V. Q. Nguyen, A. T. Pham, J. H. Park, J. E. Lee, J. K. Lee, S. Park and S. Cho, Carrier control in CuAgSe by growth process or doping, *J. Alloys Compd.*, 2021, **852**, 157094, DOI: 10.1016/j.jallcom.2020.157094.

13 H. Chen, H. Lin, Z.-X. Lin, J.-N. Shen, L. Chen and L.-M. Wu, Superionic adjustment leading to weakly temperature-dependent *ZT* values in bulk thermoelectrics, *Inorg. Chem.*, 2015, **54**, 867–871, DOI: 10.1021/ic502102e.

14 D. M. Trots, A. N. Skomorokhov, M. Knapp and H. Fuess, High-temperature behaviour of average structure and vibrational density of states in the ternary superionic compound AgCuSe, *Eur. Phys. J. B*, 2006, **51**, 507–512, DOI: 10.1140/epjb/e2006-00253-3.

15 Y. I. Aliyev, Y. G. Asadov, A. O. Dashdemirov, R. D. Aliyeva, T. G. Naghiyev and S. H. Jabarov, Polymorphic transformations and thermal expansion of some modifications in $Ag_{1.5}Cu_{0.5}Se$ and $Ag_{0.4}Cu_{1.6}Se$, *Int. J. Mod. Phys. B*, 2019, **33**, 1950271, DOI: 10.1142/S0217979219502710.

16 C. Shi, X. Xi, E. Liu, G. Wu and W. Wang, Vacancy mediated ionic mobility in a phonon glass material CuAgSe, *Solid State Ionics*, 2018, **326**, 183–187, DOI: 10.1016/j.ssi.2018.10.005.

17 S. Gahlot, E. Jeanneau, D. Singh, P. K. Panda, Y. K. Mishra, R. Ahuja, G. Ledoux and S. Mishra, Molecules *versus* nanoparticles: identifying a reactive molecular intermediate in the synthesis of ternary coinage metal chalcogenides, *Inorg. Chem.*, 2020, **59**, 7727–7738, DOI: 10.1021/acs.inorgchem.0c00758.

18 P. P. J. Helan, K. Mohanraj and G. Sivakumar, Synthesis and characterization of β-Ag_2Se and β-AgCuSe nanoparticles *via* facile precipitation route, *Trans. Nonferrous Met. Soc. China*, 2015, **25**, 2241–2246, DOI: 10.1016/S1003-6326(15)63836-5.

19 H. Z. Duan, Y. L. Li, K. P. Zhao, P. F. Qiu, X. Shi and L. D. Chen, Ultra-fast synthesis for Ag_2Se and CuAgSe thermoelectric materials, *JOM*, 2016, **68**, 2659–2665, DOI: 10.1007/s11837-016-1980-4.

20 W. Liu, X. Shi, R. Moshwan, M. Hong, L. Yang, Z.-G. Chen and J. Zou, Enhancing thermoelectric performance of $(Cu_{1-x}Ag_x)_2Se$ *via* CuAgSe secondary phase and porous design, *Sustainable Mater. Technol.*, 2018, **17**, e00076, DOI: 10.1016/j.susmat.2018.e00076.

21 G. Song, G. Li, X. Li, H. Du and F. Hu, Thermoelectric performance of copper-rich β-Cu_2Se films with Ag-doping by magnetron sputtering, *Mater. Chem. Phys.*, 2021, **260**, 124143, DOI: 10.1016/j.matchemphys.2020.124143.

22 T. Yu, S. Ning, T. Zhang, X. Chen, Q. Liu, N. Qi, Z. Chen, X. Su and X. Tang, Vacancy controlled n–p conduction type transition in CuAgSe with superior thermoelectric performance, *J. Mater. Chem. A*, 2023, **11**, 4088–4101, DOI: 10.1039/D2TA08923H.

23 E. Colacino, V. Isoni, D. Crawford and F. García, Upscaling mechanochemistry: challenges and opportunities for

sustainable industry, *Trends Chem.*, 2021, **3**, 335–339, DOI: 10.1016/j.trechm.2021.02.008.

24 P. Baláž, M. Achimovičová, E. Dutková and M. Baláž, Eccentric vibration milling for mechanochemical synthesis, in *Mechanochemistry and Emerging Technologies for Sustainable Chemical Manufacturing*, CRC Press, Boca Raton, 1st edn, 2023, pp. 215–240, DOI: 10.1201/9781003178187-13.

25 X. Zhu, C. Shi and Z. Shao, The first principle study of β-CuAgSe subcells, *J. Appl. Math. Phys.*, 2021, **9**, 1549–1559, DOI: 10.4236/jamp.2021.97106.

26 P. Baláž, *Mechanochemistry in Nanoscience and Minerals Engineering*. Berlin, Heidelberg, Springer Berlin Heidelberg, 2008, DOI: 10.1007/978-3-540-74855-7.

27 K. Gáborová, M. Achimovičová, M. Hegedüs, V. Girman, M. Kaňuchová and E. Dutková, Advantageous mechanochemical synthesis of copper(I) selenide semiconductor, characterization, and properties, *Front. Chem. Sci. Eng.*, 2022, **16**, 433–442, DOI: 10.1007/s11705-021-2066-6.

28 M. Achimovičová, M. Hegedüs, V. Girman, M. Lisnichuk, E. Dutková, J. Kurimský and J. Briančin, Mechanochemical synthesis of nickel mono- and diselenide: characterization and electrical and optical properties, *J. Nanomater.*, 2022, **12**, 2952, DOI: 10.3390/nano12172952.

29 M. Achimovičová, N. Daneu, E. Dutková and A. Zorkovská, Mechanochemically synthesized cobalt monoselenide: structural characterization and optical properties, *Appl. Phys. A*, 2017, **123**, 154, DOI: 10.1007/s00339-017-0785-9.

30 M. Achimovičová, F. J. Gotor, C. Real and N. Daneu, Mechanochemical synthesis and characterization of nanocrystalline BiSe, Bi_2Se_3 semiconductors, *J. Mater. Sci.: Mater. Electron.*, 2012, **23**, 1844–1850, DOI: 10.1007/s10854-012-0672-2.

31 S. Butt, M. U. Farooq, W. Mahmood, S. Salam, M. Sultan, M. A. Basit, J. Ma, Y. Lin and C.-W. Nan, One-step rapid synthesis of Cu_2Se with enhanced thermoelectric properties, *J. Alloys Compd.*, 2019, **786**, 557–564, DOI: 10.1016/j.jallcom.2019.01.359.

32 L. Zhu, H. Xie, Y. Liu, D. Chen, M. Bian and W. Zheng, Novel ultralong hollow hyperbranched $Cu_{2-x}Se$ with nanosheets hierarchical structure: preparation, formation mechanism and properties, *J. Alloys Compd.*, 2019, **802**, 430–436, DOI: 10.1016/j.jallcom.2019.06.237.

33 C. Fang, S. Zhang, P. Zuo, W. Wei, B. Jin, J. Wu and Y. Tian, Nanotube–nanotube transformation synthesis and electrochemistry of crystalline CuAgSe nanotubes, *J. Cryst. Growth*, 2009, **311**, 2345–2351, DOI: 10.1016/j.jcrysgro.2009.02.003.

34 S. C. Riha, D. C. Johnson and A. L. Prieto, Cu_2Se nanoparticles with tunable electronic properties due to a controlled solid-state phase transition driven by copper oxidation and cationic conduction, *J. Am. Chem. Soc.*, 2011, **133**, 1383–1390, DOI: 10.1021/ja106254h.

35 K. Chrissafis, N. Vouroutzis, K. M. Paraskevopoulos, N. Frangis and C. Manolikas, Phase transformation in CuAgSe: a DSC and electron diffraction examination, *J. Alloys Compd.*, 2004, **385**, 169–172, DOI: 10.1016/j.jallcom.2004.04.119.

36 R. Fivaz and E. Mooser, Mobility of charge carriers in semiconducting layer structures, *Phys. Rev.*, 1967, **163**, 743–755, DOI: 10.1103/PhysRev.163.743.

37 L. Tichý and J. Horák, Nonparabolicity of the conduction band and anisotropy of the electron effective mass in *n*-Bi_2Se_3 single crystals, *Phys. Rev. B*, 1979, **19**, 1126–1131, DOI: 10.1103/PhysRevB.19.1126.

38 J. Navrátil, O. Caha, J. Kopeček, P. Čermák, J. Prokleška, V. Holý, V. Sechovský, L. Beneš, K. Carva, J. Honolka and Č. Drašar, Electronic properties of Fe impurities in SnS van der Waals crystals – Revealing high-mobility holes, *Mater. Sci. Eng., B*, 2024, **301**, 117148, DOI: 10.1016/j.mseb.2023.117148.

39 B. C. Gu, Z. Li, J. D. Liu, H. J. Zhang and B. J. Ye, Effect of vacancies on thermoelectric properties of β-CuAgSe studied by positron annihilation, *Appl. Phys. Lett.*, 2019, **115**, 192106, DOI: 10.1063/1.5126899.

40 T. H. Nguyen, V. Q. Nguyen, J. H. Park, T. T. Tran, A. T. Pham, S. Park, J.-S. Rhyee and S. Cho, Raising n-type thermoelectric performance in (Te, Zn)-codoped CuAgSe, *ACS Appl. Energy Mater.*, 2023, **6**, 6151–6156, DOI: 10.1021/acsaem.3c00683.

41 Y. Jia, D. Yang, M. Zhang, H. Luo, L. Liao, Y. Zheng, B. Melzi, J. Li, Y. Liu, Y. Wang, Y. Yan and X. Tang, Dual-cation CuAgSe-based material: rapid mass transfer in synthesis and high thermoelectric performance realization, *ACS Appl. Mater. Interfaces*, 2024, **16**, 22189–22196, DOI: 10.1021/acsami.4c02217.

42 N. Fantozzi, J.-N. Volle, A. Porcheddu, D. Virieux, F. García and E. Colacino, Green metrics in mechanochemistry, *Chem. Soc. Rev.*, 2023, **52**, 6680–6714, DOI: 10.1039/d2cs00997h.